38. M. O. Scully and P. A. Lee, *ibid.* **22**, 23 (1969).
39. D. E. McCumber, *Physica (Utrecht)* **55**, 421 (1971).
40. W. C. Stewart, *Appl. Phys. Lett.* **12**, 277 (1968); D. E. McCumber, *J. Appl. Phys.* **39**, 3113 (1968).
41. R. L. Kautz, *J. Appl. Phys.* **62**, 198 (1987).
42. A. K. Jain, K. K. Likharev, J. E. Lukens, J. E. Sauvageau, *Phys. Rep.* **109**, 309 (1984).
43. R. L. Kautz, *Appl. Phys. Lett.* **36**, 386 (1980).
44. J. Clarke, in *Nonequilibrium Superconductivity, Phonons, and Kapitza Boundaries*, K. E. Gray, Ed. (Plenum, New York, 1981), pp. 353–422.
44a. A. Einstein, *Forum Century* **84**, 193 (1930).
45. R. L. Kautz, *Phys. Lett.* **125**, 315 (1987).
46. B. N. Taylor and T. J. Witt, *Metrologia* **26**, 47 (1989).
47. G. Feinberg and M. Goldhaber, *Sci. Am.* **209**, 36 (October 1963).
48. G. J. Sloggett, W. K. Clothier, B. W. Ricketts, *Phys. Rev. Lett.* **57**, 3237 (1986).
49. The author acknowledges with gratitude the comments of B. N. Taylor, J. E. Lukens, C. A. Hamilton, R. L. Kautz, and H. B. McDonald during the preparation of this article.

Research Article

Imaging Surface Atomic Structure by Means of Auger Electrons

DOUGLAS G. FRANK, NIKOLA BATINA, TERESA GOLDEN, FRANK LU, ARTHUR T. HUBBARD*

Measurements of the complete angular distribution of Auger electrons emitted from well-defined platinum[111] single-crystal surfaces have led to the discovery that the distributions are composed of "silhouettes" of surface atoms "back lit" by emission from atoms deeper in the solid. Theoretical simulations of Auger electron angular distributions based upon atomic point emitters and spherical atomic scatterers of uniform cross section are in close agreement with these experimental results, but opposite to previous theoretical predictions. In view of the definitive results obtained and the straightforward agreement between theory and experiment, angular distribution Auger microscopy (ADAM) is useful for direct imaging of interfacial structure and investigation of electron-solid interactions in the physical and biological sciences and engineering. Applicability of ADAM is illustrated by images obtained for monolayers of silver and iodine on platinum[111].

EXCITATION OF AN ATOM, SUCH AS BY A FAST-MOVING electron or x-ray, can result in the removal of a core electron, followed by a relaxation process in which an outer electron fills the core vacancy and a third electron, an "Auger electron," is ejected from the atom. Auger electrons were first recognized by Pierre Auger in cloud chamber experiments (*1*), and were found to have discrete energies characteristic of the emitting elements. Auger electron spectroscopy has since found wide application for elemental identification and analysis (*2*). In the course of that work, Auger signals from solid samples were found to vary significantly with the direction of emission from the surface (*3, 4*). Based upon relatively limited data, these variations have been mistakenly attributed to anisotropic emission from individual atoms, to diffraction, to multiple scattering or to a combination of these effects (*5–20*). In an effort to more clearly understand the nature of Auger electron angular distributions, we designed and constructed instrumentation capable of measuring Auger emission over the full range of angles above a solid surface. The resulting observations reveal that the measured angular distribution contains the "silhouettes" of near-surface atoms "back lit" by Auger emission originating from atoms deeper in the solid.

Theoretical simulations based upon isotropic Auger electron emission from atomic point-emitters and scattering by spherical atomic scatters of uniform cross section are in close agreement with the measured angular distributions. Best agreement occurred when the radii of the scatterers were taken to be 60 to 90 percent of their atomic radii, and the scatterers were 40 percent transparent.

Other mechanisms, such as anisotropic emission, diffraction, or multiple scattering, are not needed to explain the observed results. These experimental and theoretical findings reveal the potential usefulness of such measurements, which we have termed "angular distribution Auger microscopy" (ADAM), as a tool for imaging atomic and molecular structure at interfaces, as well as a means by which to study the interaction of electrons with matter.

Measurement of Auger electron angular distributions. The experimental apparatus employed for ADAM is illustrated in Fig. 1A (*21*). The measurements were performed in an ultrahigh vacuum chamber operated at a pressure below 10^{-7} pascal (10^{-12} atm) to preserve sample cleanliness and to permit the unobstructed travel of electrons. To stimulate Auger emission, a 3-mm^2 portion of the sample was irradiated with a 4-μA electron beam at 2000-eV kinetic energy, impinging on the [111] plane at 79° from the surface normal (toward the [001] plane). (Smaller beam currents should be used with samples sensitive to beam damage.) The resulting Auger emission (65 eV) was angle-resolved (±0.7°) with the use of collimating apertures. Energy resolution was accomplished by means of an electrostatic analyzer; the electrons passing through the energy analyzer were modulated with an amplitude equivalent to ±10 eV at a frequency of 1 kHz, amplified, counted, synchronously

The authors are in the Surface Center and Department of Chemistry, University of Cincinnati, Cincinnati, OH 45221.

*To whom correspondence should be addressed.

detected by means of a lock-in amplifier (*22*) and digitized, and then transferred to computer memory (*23*).

The complete data set for the angular distribution (Fig. 2) was gathered during a single 2-hour time period. Data were gathered by scanning the β angle of detection from 20° to 160° for each α setting, and α was stepped in 1° increments (Fig. 1). The Auger signal intensity was digitized every 0.1° in β, producing 1410 values per α setting. These 1410 data points were then reduced to 141 points at 1° intervals by boxcar averaging in groups of ten. Thus, the final angular distribution contained 18,471 data points, one value per degree in α and β. Data were displayed in real time and also stored for later examination.

The platinum single crystal we used (*24*) was oriented by means of x-ray reflection (Laué) photography (*25*), cut, polished (*26*), and etched with aqua regia. The crystal was then placed in the ultrahigh vacuum chamber, and all of its faces were simultaneously cleaned by bombardment with argon ions (*27*), followed by annealing at ~800°C to produce a highly ordered platinum[111] (Pt[111]) surface of known spatial orientation. Atoms of the Pt[111] surface are close packed in a hexagonal arrangement. Platinum has a cubic close-packed structure consisting of these hexagonal layers arranged in a repeating (ABCABC . . .) manner (*28*). Surface order and cleanliness were verified by low-energy electron diffraction (LEED) (*29*) and Auger electron spectroscopy (*2*), respectively. Of course, the ADAM experiment itself constitutes an independent verification of cleanliness.

Platinum has numerous Auger transitions ranging in energy from 11 to 78,389 eV (*30*). Naturally, the strongest transitions give the best ADAM images. Accordingly, for this study the strong Auger emission near 65 eV (produced by several overlapping transitions, particularly $O_2O_{4,5}O_{4,5}$, $N_7O_{4,5}O_{4,5}$, and $N_6O_{4,5}O_{4,5}$) was chosen because it provides a low-energy, high-intensity signal, resolvable from other transitions. Low-energy electrons generally have the largest scattering cross sections, and therefore afford the best surface sensitivity and the least complicated results. The kinetic energy distribution of electrons emanating from Pt[111] along the surface normal is shown in Fig. 1B (top curve). Because the energy distribution of an Auger process is narrower than that of background, differentiation is commonly used to emphasize the Auger signals, Fig. 1B. A broad maximum occurs near 40 eV due to "secondary electrons" produced by various inelastic processes. The elastic reflection peak is barely visible at the primary energy (1000 eV). The Auger process near 65 eV is visible after differentiation of the energy spectrum (Fig. 1B, middle curve). Angular distributions for Pt[111] were obtained by tuning to the negative inflection of the differentiated spectrum. Integration of the energy spectrum (Fig. 1B, bottom curve), shows that elastic reflection amounts to only about 4 percent of the total reflected intensity. Analogously, for an Auger electron traveling through platinum, only about 4 percent of the scattering events are elastic, including diffraction. Indeed, this preponderance of inelastic scattering over elastic scattering and diffraction is one of the attributes that makes ADAM a potent method for direct imaging of surface atomic structure.

Angular distribution from a crystalline surface. Shown in Fig. 2 is the experimental angular distribution of Auger electrons emitted from a Pt[111] surface with a kinetic energy of 65 eV. Regions of highest intensity appear white; lowest are black (less than 10 percent of full scale) (Fig. 2A). The contour map (Fig. 2B) may be helpful in locating the spherical coordinates of the features. Highest intensity is observed perpendicular to the [111] surface (center of the distribution, $\phi = 0°$). Other intense features are present along the $\theta = 90°$, 210°, and 330° directions near $\phi = 13°$ and 31°. Less intense maxima are seen along the $\theta = 30°$, 150°, and 270° directions. In preparing Fig. 2, we took advantage of the threefold symmetry of the distribution to perform threefold averaging of the data. Data were not obtainable in a narrow region near $\theta = 270°$ for ϕ greater than 57° because this region was occupied by the incident beam. Auger intensity steadily decreases and becomes relatively featureless near the edges of the distribution ($\phi > 70°$) because the distance that the electrons must travel through the solid increases as grazing angles of emission are approached.

Simulation of angular distribution from platinum [111]. An immediate consequence of measuring and displaying a *complete* angular distribution, Fig. 2, is that the characteristics of the distribution are readily visualized. The distribution from Pt[111] is recognizable as a hexagonal layer of atomic scatterers back lit by point sources located below the layer. That is, the data suggest that the angular distribution is created by Pt atoms behaving as spherical scatterers illuminated from underneath by other Pt atoms acting as point sources. The basic geometry of the situation indicates that emission from the first four Pt[111] layers predominates (Fig. 3, A to D). Since the observed silhouettes do not display nearly uniform density (Fig. 2), the scatterers are evidently quite uniform from center to edge. Digital simulations of the angular distribution consistent with these principles showed best quantitative agreement between theory and experiment when each individual scatterer was

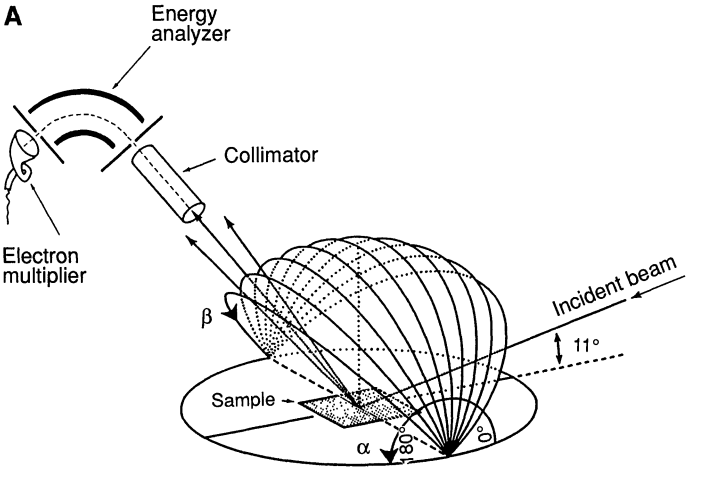

Fig. 1. (**A**) ADAM angular distributions are measured versus the angular coordinates (α and β) of the detector. Auger electron emission is stimulated by an incident electron beam impinging on the sample at a fixed angle (11° from the surface plane). An Auger electron traveling along the selected trajectory (α, β) must pass through the angle-resolving collimator and an energy-resolving analyzer before being amplified and counted. (**B**) Kinetic energy distribution of electrons detected at the Pt[111] surface normal when beam of electrons (1000 eV) is incident at 11° from the surface plane. The count rate of electrons versus energy at a resolution of 10 eV (top curve) displays a prominent peak at 20 eV, resulting primarily from inelastic scattering processes, although barely perceptible fluctuations in slope are present due to Auger processes. A barely noticeable peak at 1000 eV is due to elastic scattering of the incident electrons. The middle curve is the derivative of the electron kinetic energy distribution (top curve) with respect to kinetic energy, which emphasizes the relatively narrow energy distributions due to Auger processes and elastic scattering. The Auger process near 65 eV was used to image Pt[111] in this study. The bottom curve results from integration of the electron kinetic energy distribution (top curve), and indicates that only about 4 percent of electron reflection is elastic.

40 percent transparent and had a radius equal to 90 percent of the atomic radius. For example, Fig. 3B shows the predicted distribution of Auger electrons emitted from Pt atoms in the second layer as scattered by Pt atoms in the top layer. The flux of Auger electrons is greatest where the path of emission passes through gaps in the top layer. Deepest shadows are seen where the trajectory encounters more than one scatterer, such as near the edge of the distribution. Figure 3, C and D, shows the distributions expected for emitters located two and three layers below the scattering layer, respectively.

In the observed angular distribution of Auger electrons from Pt[111] (Fig. 2), all Pt atoms near the surface act as emitters and scatterers. Accordingly, the simulation multiplies the attenuations due to each scatterer encountered along the path to the detector (S_j) by the emission originating from each atom (ϵ^{i-1}), and sums the contributions from all layers (i) of atoms (Eq. 1):

$$I(\theta, \phi) = \epsilon^0 S_0(\theta, \phi) + \epsilon^1 S_0(\theta, \phi) S_1(\theta, \phi) + \ldots = \sum_{i=1}^{N} \epsilon^{i-1} \prod_{j=0}^{i-1} S_j(\theta, \phi) \quad (1)$$

More specifically, $I(\theta, \phi)$ is the resulting angular distribution of Auger intensity, θ and ϕ are spherical coordinates of the path of emission ($\phi = 0°$ along the surface normal), ϵ^{i-1} is proportional to the intensity of the incident beam as it reaches the i^{th} layer (ϵ is the incident beam attenuation factor per layer; $\epsilon = 1$ in the present work) and $S_j(\theta, \phi)$ describes the scattering cross section for an emitter-to-scatterer separation of j layers along the path defined by θ and ϕ. In our study, 16 Pt[111] layers were included in the simulation on the basis of the finding that the contributions due to emitters located in deeper layers had a negligible effect on the calculated distribution. The theory has a relatively simple form for a cubic close-packed metal such as Pt (Eq. 1) because all of the atomic emitters and scatterers are crystallographically equivalent. The simulated angular distribution, $I(\theta, \phi)$, from Pt[111] is shown in Fig. 3E.

The observation that electron scattering probability is virtually independent of the path through an atom is consistent with the generally accepted theory of electron scattering described by Gryzinski (*31*): tightly bound electrons have very small cross sections (1 percent) compared with electrons in outer shells (99 percent). In other words, the bound electrons scattering Auger electrons with greatest efficiency are most abundant near the perimeter of the scatterer. The larger density of outer-shell electrons near the perimeter compensates for the corresponding decrease in path length through the atom (Fig. 4A). Consequently, the angular distribution is determined by the number of scatterers encountered along the path to the detector and not simply by the distance traveled through the solid.

Atomic vibration is expected to affect ADAM experiments, as the amplitude of thermal vibration is about 9 percent of the atomic radius at room temperature (*32*), although the simulation depicted in Fig. 3E did not include vibrations. Vibration has been introduced into the simulation by varying the coordinates of the emitters and scatterers, (Eqs. 2 and 3 and Fig. 4B).

$$\Delta\theta = \arctan [\Delta r/(d \tan \phi)] \quad (2)$$

$$\Delta\phi = \arctan [(\Delta r \cos \phi)/d] \quad (3)$$

That is, the effect of thermal vibration is simulated by averaging the individual scattering cross sections, $S_j(\theta, \phi)$, over a small range of angles defined by $\Delta\theta$ and $\Delta\phi$. Obviously, vibration affects the angular distribution most when the emitter and scatterer are closest together. A simulation that includes ±9 percent vibrational motion of emitters and scatterers is shown in Fig. 5A, which can be compared with the vibrationless calculation shown in Fig. 3E. Sharper angular distributions are expected at temperatures approaching absolute zero (*33*). Vibrational amplitudes of surface atoms are expected to be about 25 percent larger than those of bulk atoms (*29*) and of non-uniform distribution in space, although for simplicity in our analysis all atoms were assigned identical spherical amplitudes. The excellent agreement between simulation and experiment is demonstrated in Fig. 5B, which superimposes contour lines of the experimental data (Fig. 2) onto the simulated color map shown in Fig. 5A.

The specific emitter-to-scatterer geometric relation giving rise to the various features (silhouettes) of the experimental distribution can be recognized by comparing simulations with experimental data (Fig. 5, C to E). Contours represent calculated Auger intensities from Fig. 3, B to D, superimposed on the experimental angular distribution shown in Fig. 2. For example, the Y-shaped bright region at the center of the distribution arises from interatomic gaps in the layer immediately above the emitter (Fig. 5C). Bright spots arranged hexagonally near the center of the distribution ($\phi = 12°$) are primarily due to emission from the fourth layer followed by scattering by the top layer (and other such combinations in which the separation is three layers, Fig. 5E). Features located toward the outer edges of the pattern ($\phi > 45°$) are primarily due to 1:2 and other combinations of adjacent emitters and scatterers for which the trajectory encounters more than one scatterer per layer.

ADAM images of surface layers. Usefulness of ADAM for imaging the structure of surface atomic layers is illustrated by results obtained for a silver (Ag) monoatomic layer having an overlayer of iodine (I) atoms, all resting atop the Pt[111] surface described above. [Preparation of the layers has been described (*33, 34*).] Presented here is direct evidence concerning their structure. The angular distribution of Ag Auger electrons (355 eV, primarily the $M_5N_{4,5}N_{4,5}$ and $M_4N_{4,5}N_{4,5}$ transitions) displays the silhouettes of the overlying I atoms, as expected (Fig. 6A). The dark Y-shaped region of Fig. 6A is due to the small Pt signal of opposite sign at 355 eV (primarily $N_3N_7N_7$). However, the I angular distribution (507 and 518 eV, $M_5N_{4,5}N_{4,5}$ and $M_4N_{4,5}N_{4,5}$ transitions) is essentially featureless because I is the outermost layer (Fig. 6B).

That I atoms are located atop some of the Ag atoms is evident from the round silhouette in the center of Fig. 6A. Hexagonal arrangement of neighboring I atoms is apparent from the gaps and shadows nearer the perimeter of the image. A model having these characteristics appears in Fig. 6C. A simulation of the angular distribution of Ag Auger electrons based upon this model, formulas analogous to Eq. 1, the same attenuation as for Pt, an I scattering radius of 0.80 Å and including atomic vibrations of 35 percent of the Ag–I distance is shown in Fig. 7A. Data are compared with theoretical contours in Fig. 7B.

Quantitative use can be made of the ADAM data to obtain interatomic distances and directions. Only simple trigonometry, prompted by the simulations, is required. For example, the Ag–Ag distance in Fig. 7, A and B, is 2.98 ± 0.07 Å, compared with 2.88 Å reported for Ag metal (*28*). The Ag–I distance is 2.40 ± 0.12 Å, compared with 2.80 Å in tetrahedral AgI (zinc blende structure) (*28*). Note that the monolayer Ag–Ag distance is about 7 percent greater than the Pt–Pt distance (2.776 Å) in Pt metal (*28*).

Theoretical considerations. Although successfully explaining the angular distributions reported here, and conforming to the basic principles of electron scattering (*31*), our simple model contradicts the predictions of previous theories for Auger electron angular distribution. Included among the contradicted theories are those invoking anisotropic Auger electron emission from individual atoms, diffraction, or multiple elastic scattering of Auger electrons, the lensing effect (also termed the searchlight effect or forward scatter-

ing) (*5–20, 35*), or some combination of these effects. There are compelling reasons why those explanations did not predict the observed behavior. First, Auger electron emission from each individual atom is essentially isotropic. This is demonstrated by the Auger emission from a layer of I atoms atop a Ag monolayer, Fig. 6B: the I Auger angular distribution is essentially featureless. On the basis of our results, we expect that other elements behave similarly to iodine in this respect. Second, Auger electrons, unlike photoelectrons (*36*), are emitted at random times preventing formation of the plane waves required for efficient diffraction. In particular, the cross sections for elastic scattering of Auger electrons are very small and thus contribute very little to the observed angular distribution,

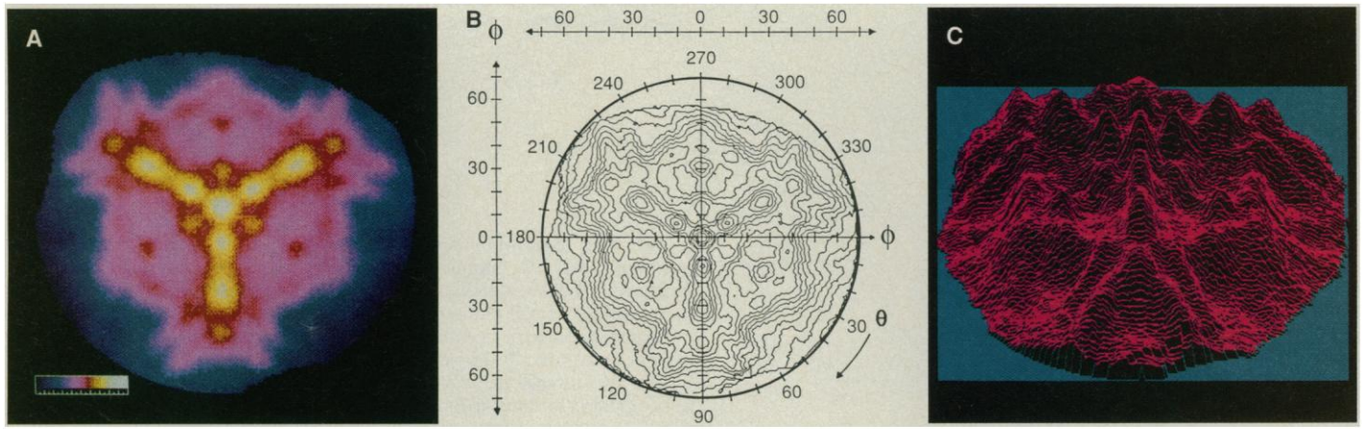

Fig. 2. The measured angular distribution of Auger electrons (65-eV kinetic energy) emitted from a bare Pt[111] surface displays striking variations in signal with angle of detection. Bright colors in (**A**) denote large Auger signals as indicated by the scale at lower left. Features of the angular distribution are due to the "silhouettes" of surface atoms located between emitting atoms and the detector. Each layer of Pt is hexagonally close packed, and the cubic close-packed structure of Pt places the layers so as to produce the observed threefold symmetry, as illustrated in Fig. 3. Data were averaged with the use of this threefold symmetry. Electrons were not collected at angles occupied by the incident electron beam (top edge of distribution). These same angular distribution data are depicted in a contour map (**B**) and in a relief map (**C**). Scales in (B) show spherical coordinates that also apply to (A), (C), and all other distributions shown.

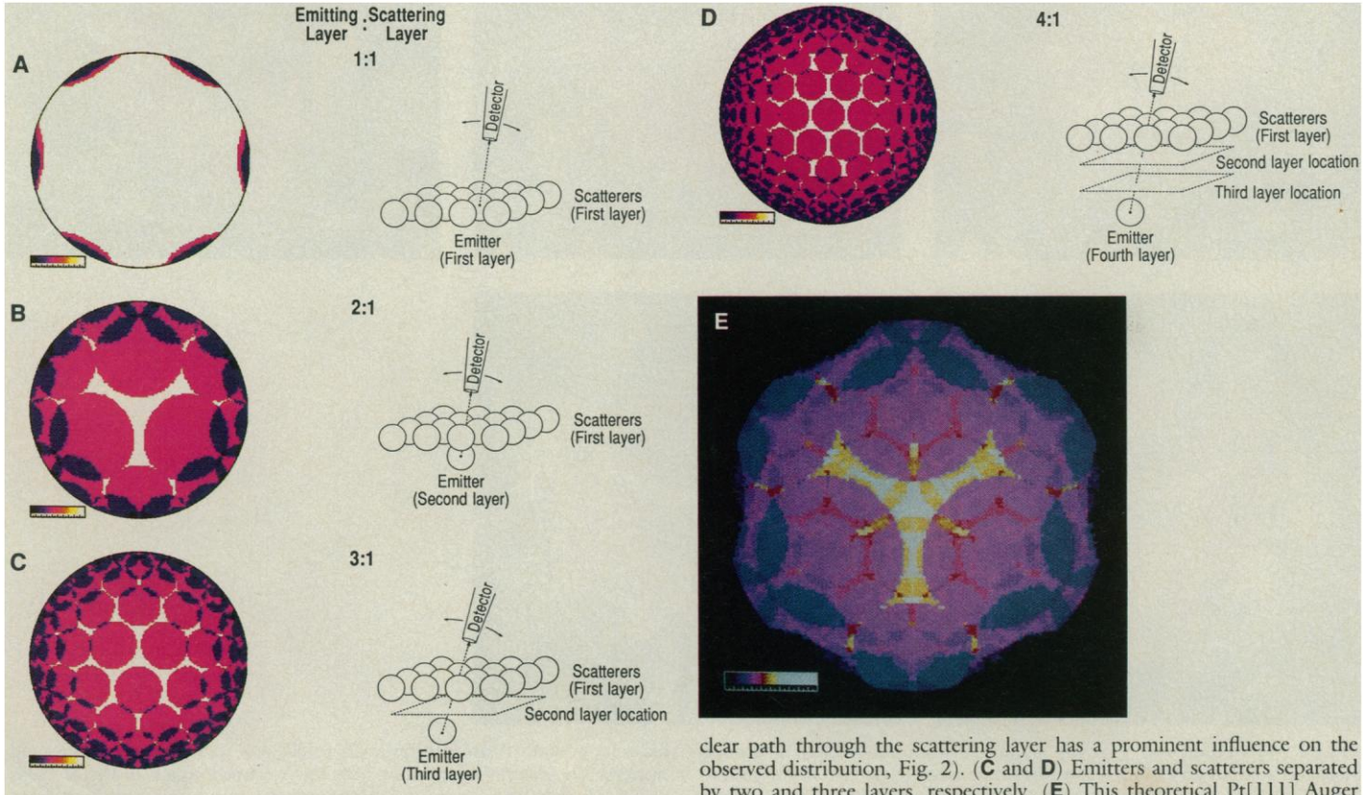

Fig. 3. Theoretical angular distributions (layer-by-layer) illustrate how "silhouettes" result when Auger electrons from atomic point emitters are scattered by spherical atoms of uniform cross section and radii equal to 90 percent of the interatomic distance. (**A**) Emitters and scatterers all in the same layer. (**B**) Emitters and scatterers in adjacent layers. (The Y-shaped clear path through the scattering layer has a prominent influence on the observed distribution, Fig. 2). (**C** and **D**) Emitters and scatterers separated by two and three layers, respectively. (**E**) This theoretical Pt[111] Auger electron angular distribution was calculated by considering all Auger emission and scattering events occurring in the outermost 16 atomic layers. It is dominated by contributions from the top four layers, shown in (A) to (C). Attenuations due to scattering were multiplied and intensities due to layers of emitters were added as specified in Eq. 1.

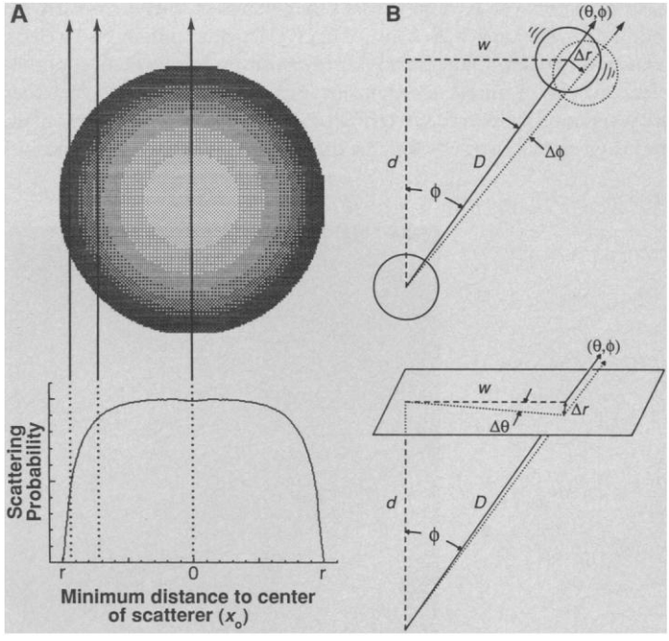

Fig. 4. (**A**) Auger electron angular distributions exhibit atomic silhouettes that are virtually uniform from center to edge. Evidently, the probability that an Auger electron will be scattered is nearly independent of the trajectory through the atom. This uniformity of scattering probability $P(x_0)$, versus distance from the center of the atom, x_0, can be understood in terms of an approximately linear increase in the outer shell electron density, $\rho(y)$, from about 40 percent at the center of the atom to 100 percent at the perimeter. This increase in density compensates for the shorter travel, $2y_0$, nearer the perimeter. Outer-shell electron density is responsible for nearly all inelastic scattering of Auger electrons (*31*). The density function illustrated is based upon the following equations:

$$P(x_0) = \int_{-y_0}^{y_0} \rho(y)dy$$

where

$$y_0 = (r^2 - x_0^2)^{1/2} \text{ and } \rho \approx 4 + \sum_{n=1}^{6} \left(\frac{x_0^2 + y^2}{r^2}\right)^{n/2}$$

and r is the radius of the scatterer, which ranges from 60 to 90 percent of the atomic radius. (**B**) Atomic vibrations are expected to affect measured Auger electron angular distributions and can be simulated by averaging the influences of small random fluctuations, $\Delta\phi$ (top) and $\Delta\theta$ (bottom) in the theoretical trajectories defined by (θ, ϕ). Δr is the amplitude of the vibration (9 percent of the Pt–Pt platinum distance; 35 percent of the Ag–I distance). D is the distance between the emitter and the scatterer; d and w are the vertical and horizontal components of D, respectively.

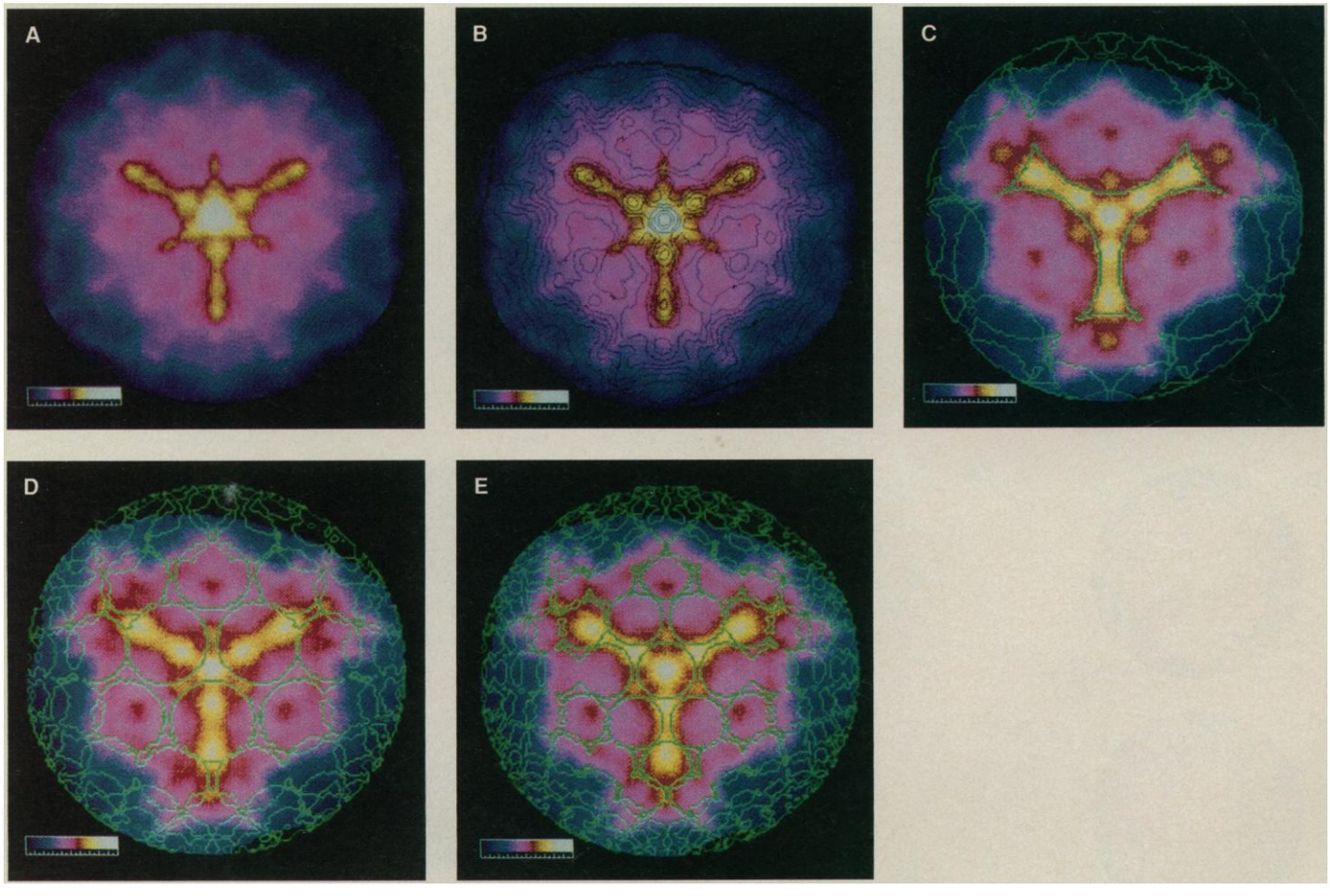

Fig. 5. (**A**) Theoretical Pt[111] angular distribution including atomic vibration amplitudes expected at room temperature (9 percent of the atomic radius). The effect of uniform vibration of all atoms in the first 16 layers can be seen by comparing (A) with Fig. 3E, which was calculated assuming no atomic vibration. The extent of agreement between experiment and theory can be seen in (**B**), where contour lines (black) corresponding to the experimental data shown in Fig. 2 are added to (A). Theoretical contour lines (green) from Fig. 3, B to D, are compared with the experimental data to illustrate how observed features arise. In (**C**), contours due to emitters and scatterers in adjacent layers show how the Y-shaped region in the center is produced. Adjacent layer interactions are the most frequently occurring emitter-scatterer combinations, hence their prominence in the distribution. (**D**) Contours due to emitters and scatterers in alternate layers, showing how the smaller, inverted "Y" results. (**E**) The small hexagon of spots in the center of the distribution is produced by emitters and scatterers three atomic layers apart.

as noted from the data in Fig. 1B. This situation is illustrated in Fig. 7C. Multiple elastic scattering is of course even less probable, decreasing approximately as $(1/25)^N$. The "searchlight effect" explanation (*35*) (according to which atoms neighboring the emitter redirect electrons elastically, focusing them along the internuclear axes) did not predict the observed results, but rather the opposite. In summary, although the outcomes of Auger electrons are undoubtedly numerous, our data demonstrate that most Auger electrons simply undergo inelastic scattering by atoms located along their path.

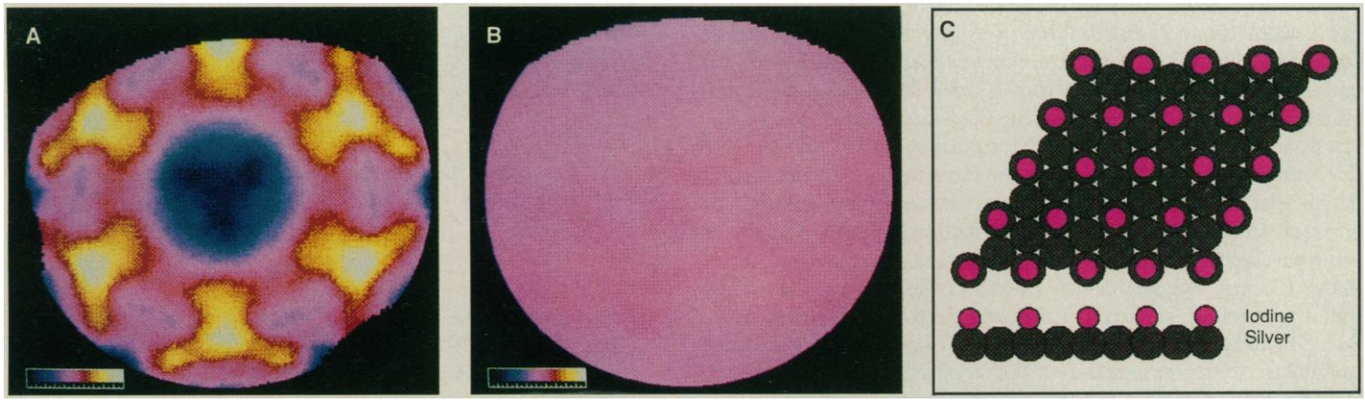

Fig. 6. Measured angular distributions of (**A**) 355-eV Ag Auger electrons and (**B**) 507- and 518-eV I Auger electrons obtained from Ag and I atomic layers on a Pt[111] surface illustrate the usefulness of ADAM for structural characterization of surface layers deposited epitaxially. Electroplating of Ag and adsorption of I monolayers is described in (*34*). Clearly visible at the center of the Ag Auger distribution (A) is the round silhouette of the overlying I atom; neighboring I atoms form the surrounding hexagonal pattern. The location, dimensions, and density of the central silhouette in (A) indicate that each I atom is located atop an Ag atom, as illustrated in (C). Note that the I Auger angular distribution (B) is essentially featureless, as expected since iodine forms the outermost layer. (**C**) Electroplating of silver onto an iodine-pretreated Pt[111] surface (*34*) produces structures composed of hexagonal monolayers of Ag atoms. Pretreatment of the Pt surface with iodine (I^- or I_2) leads to an ordered overlayer of I atoms which remains strongly attached to the outermost Ag layer during plating. The structure shown here represents the second of four successive stages of plating: (i) Ag sub-monolayer; (ii) Ag monolayer, (iii) two Ag monolayers; and (iv) a crystalline Ag film. ADAM data indicate that the Ag–Ag interatomic distance is 7 percent larger than the Pt–Pt distance. The I atoms are located atop one-third of the Ag atoms in the "$(\sqrt{3} \times \sqrt{3})R30°$" arrangement shown. The I–I interatomic distance is 20 percent greater than the van der Waals radius of closest approach.

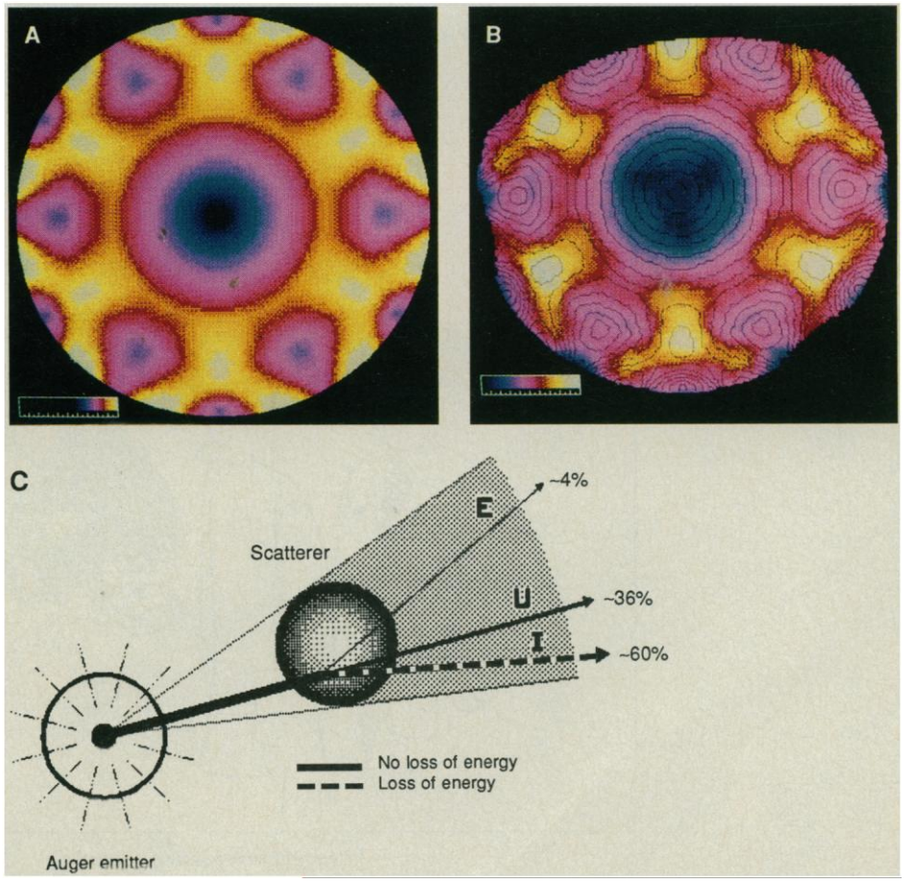

Fig. 7. Theoretical Auger electron angular distribution (**A**) for a Ag monolayer with I atoms atop, as shown in Fig. 6C. The theoretical distribution, shown as contour intervals in (**B**), predicts the measured distribution from Fig. 6A. (**C**) Auger electron emission from each individual atom is isotropic, as demonstrated by the data in Fig. 6B. The features of Auger electron angular distributions, such as Figs. 2 and 6, result primarily from inelastic scattering by atoms located between emitting atoms and the detector. The sharpness of the silhouettes and other basic characteristics of the distributions reveal that atoms behave as point emitters of Auger electrons. Scattering probability is nearly uniform for all trajectories through the atom, evidently because the outer-shell electrons (which do most of the scattering) are concentrated near the perimeter of the atom (see Fig. 4A). Scattering radii range from 60 to 90 percent of the corresponding atomic radii. About 60 percent of the Auger electrons passing through an atom are scattered inelastically and thus are energy resolved from the Auger signal. About 36 percent pass through the atom unaffected, while about 4 percent are scattered elastically and are detected at other analyzer positions.

Conclusions. Measurements of Auger electron angular distributions from well-defined Pt[111] single-crystal surfaces have led to the discovery that the distributions consist primarily of the silhouettes of near-surface atoms back lit by Auger emission originating from atoms deeper in the metal. Auger electron angular distribution schemes based upon anisotropic emission, multiple scattering, diffraction, focusing by neighbor atoms, and other effects are not required to account for these results. Measurement and display of the *complete* angular distribution of Auger electrons has greatly facilitated recognition of the experimental features. Auger electron emission (65 eV) observed from a bare Pt[111] single-crystal surface originates primarily from the outermost four to five atomic layers, and therefore affords optimal surface sensitivity and simplicity. A theoretical simulation of this situation based upon emission of Auger electrons from atomic point sources and scattering by spherical atoms is in close agreement with experiment. In view of these developments in theory and experiment, the measurement of Auger electron angular distributions (ADAM) is expected to be useful for probing surface structure and electron-solid interactions. ADAM images of monolayers of Ag and I have demonstrated this usefulness. Other potential areas of application include: organic layer structures; molecular conformations; atomic vibrations; mineral, metal, and material interfacial structures; and characterization of thin-films or epitaxial layers produced by physical, chemical, or electrochemical procedures.

REFERENCES AND NOTES

1. P. Auger, *Ann. Phys. (Paris)*, **6**, 183 (1926); *Surf. Sci.* **48**, 1 (1975).
2. M. T. Thompson, M. D. Baker, A. Christie, J. F. Tyson, *Auger Electron Spectroscopy* (Wiley, New York, 1985); J. A. Schoeffel and A. T. Hubbard, *Anal. Chem.* **49**, 2330 (1977); J. L. Stickney, S. D. Rosasco, D. Song, M. P. Soriaga, A. T. Hubbard, *Surf. Sci.* **130**, 326 (1983); N. Batina *et al.*, *Electrochim. Acta* **34**, 1031 (1989).
3. L. A. Harris, *Surf. Sci.* **15**, 77 (1969).
4. S. A. Chambers, H. W. Chen, S. B. Anderson, J. H. Weaver, *Phys. Rev. B* **34**, 3055 (1986), and references therein.
5. S. J. White, D. P. Woodruff, L. McDonnell, *Surf. Sci.* **72**, 77 (1978).
6. R. Baudoing, E. Blanc, C. Gaubert, Y. Gauthier, *ibid.* **128** (no. 1), 22 (1983), and references therein.
7. T. Matsudaira and M. Onchi, *J. Phys. Chem.* **12**, 3381 (1979), and references therein.
8. D. M. Zehner, J. R. Noonan, L. H. Jenkins, *Phys. Lett. A.* **62A**, 267 (1977).
9. H. L. Davis, and T. Kaplan, *Solid State Commun.* **19**, 595 (1976); H. L. Davis, *Proc. 7th Int. Vac. Congr.* **3**, 2281 (1977).
10. J. W. Gadzuk, *Surf. Sci.* **60**, 76 (1976).
11. S. P. Weeks and A. Liebsch, *ibid.* **62**, 197 (1977).
12. M. M. El Gomati, J. P. Broomfield, J. A. D. Mathew, M. Prutton, *Scanning Electron Microsc.* **3**, 1101 (1983).
13. H. Hilferink, E. Lang, K. Heinz, *Surf. Sci.* **93**, 398 (1980).
14. J. M. Plociennik, A. Barbet, L. Mathey, *ibid.* **102**, 282 (1981).
15. B. M. Duc, *Vide Couches Minces* **205**, 151 (1981).
16. T. Koshikawa, T. Von dem Hagen, E. Bauer, *Surf. Sci.* **109**, 301 (1981).
17. E. C. Goldberg and J. Ferron, *ibid.* **172**, L523 (1986).
18. W. O. Barnard, H. C. Snyman, F. D. Auret, *S. Afr. J. Phys.* **10**, 153 (1987).
19. G. M. Mikhailov *et al.*, *J. Electron Spectros. Relat. Phenom.* **46**, 145 (1988).
20. A. Mroz, S. Mroz, M. Zagorski, *Surf. Interface Anal.* **12**, 49 (1988).
21. ADAM, 3793 Fox Run Drive, Cincinnati, OH 45236.
22. EG&G, Princeton Applied Research, P.O. Box 2565, Princeton, NJ 08540.
23. Hewlett-Packard, 19310 Pruneridge Avenue, 49A, Cupertino, CA 95014.
24. Johnson-Matthey, P.O. Box 1087, Seabrook, NH 03874.
25. E. A. Wood, *Crystal Orientation Manual* (Columbia Univ. Press, New York, 1963).
26. L. E. Samuels, *Metallographic Polishing by Mechanical Methods* (Pitman, London, 1967).
27. G. Carter and J. S. Colligon, *Ion Bombardment of Solids* (Elsevier, Amsterdam, 1975), pp. 223–273.
28. L. Pauling, *The Nature of the Chemical Bond* (Cornell Univ. Press, New York, ed. 3, 1960).
29. L. J. Clarke, *Surface Crystallography: An Introduction to Low-Energy Electron Diffraction* (Wiley, New York, 1985).
30. W. A. Coghlan and R. E. Clausing, *At. Data* **5**, 317 (1973).
31. M. Gryzinski, *Phys. Rev. A.* **138**, 305 (1965); *ibid.*, p. 322; *ibid.*, p. 336.
32. C. A. Wert and R. M. Thomson, *Physics of Solids* (McGraw-Hill, New York, 1964), pp. 34–43.
33. D. G. Frank *et al.*, *J. Phys. Chem.*, in press.
34. A. Wieckowski, B. C. Schardt, S. D. Rosasco, J. L. Stickney, A. T. Hubbard, *Surf. Sci.* **146**, 115 (1984), and references therein.
35. W. F. Egelhoff, Jr., *J. Vac. Sci. Technol. A.* **3**, 1511 (1984).
36. C. S. Fadley, *Prog. Surf. Sci.* **16**, 275 (1984).

37. We gratefully acknowledge the support of the National Science Foundation, the Air Force Office of Scientific Research, Pratt & Whitney, and the technical assistance of A. Case, F. Douglas, D. Hurd, J. Rovang, and R. Shaw.

13 September 1989; accepted 28 November 1989

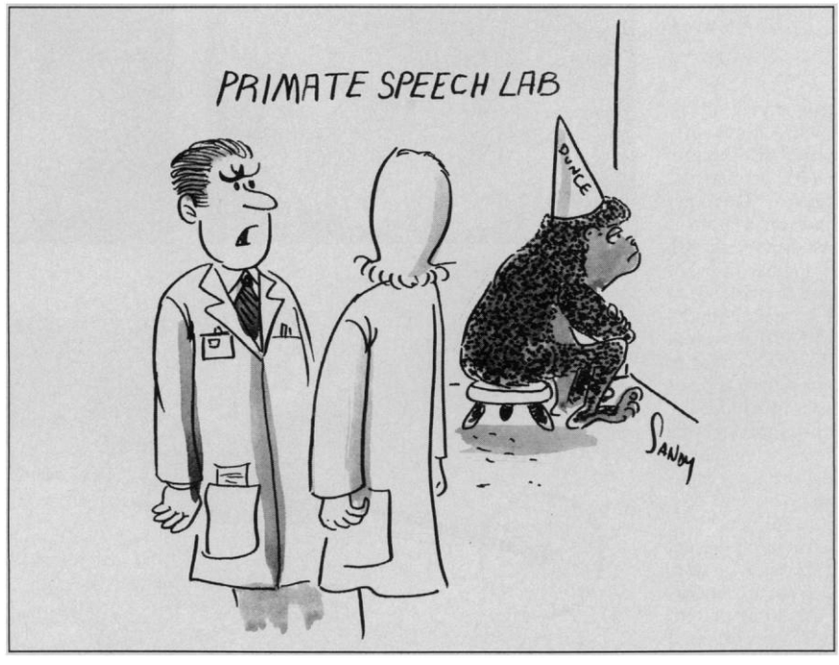

"I caught him passing notes."